Available online at www.sciencedirect.com

ScienceDirect

Advances in Space Research 69 (2022) 3350–3361

ADVANCES IN SPACE RESEARCH (a COSPAR publication)

www.elsevier.com/locate/asr

Effects of particle precipitation on the polar mesospheric summer echoes observed by EISCAT VHF 224 MHz radar

Viswanathan Lakshmi Narayanan [a,*], Ingemar Häggström [b], Ingrid Mann [a]

[a] Department of Physics and Technology, UiT The Arctic University of Norway, Tromsø, Norway
[b] EISCAT Scientific Association, Kiruna, Sweden

Received 21 October 2021; received in revised form 10 February 2022; accepted 10 February 2022
Available online 23 February 2022

Abstract

We present the results from investigation of spectra of polar mesospheric summer echoes (PMSE) observed with EISCAT VHF 224 MHz radar during energetic particle precipitation events in the summer of 2019. We used the sudden enhancements in electron densities derived from the VHF observations above 90 km as indicators of particle precipitation. We find that the altitude extent of the PMSE increased along with an enhancement of the strength of the pre-existing PMSE. On some occasions, PMSE suddenly appeared during particle precipitation events. After the particle precipitation subsided, the PMSE intensities continued to be stronger for a few minutes and then decreased. At the altitudes where the maximum enhancement in PMSE backscatter occurred, there is no corresponding broadening in the spectral widths. Interestingly, the most intense PMSE echoes almost always coincided with the lower values of spectral widths both during particle precipitations and other times. In some cases, the spectral widths show well separated regimes between the upper and lower parts of the PMSE layers and this also happened irrespective of particle precipitation. The frequency Doppler shifts showed alternating upward and downward motions without much difference before and after the particle precipitation. Based on these observations, we conclude that the sudden enhancement in the electron densities during particle precipitation intensifies PMSE structures that match the Bragg scale of the incident radio wave thereby enabling an enhancement in the backscatter strength. Similarly, PMSE backscattering may get initiated in the altitudes in which the structures were already present but where electron density was not sufficient before the onset of precipitation. Spectral widths and Doppler velocities does not show sudden variations with particle precipitation because they depend on the neutral dynamics.

Keywords: Polar mesospheric summer echoes; Particle precipitation; VHF radar; Spectral width

1. Introduction

Polar Mesospheric Summer Echoes (PMSE) are intense radar echoes observed from the upper mesospheric region, typically between 80 and 90 km during summer times in the high latitudes (Czechowsky et al., 1979; Ecklund and Balsley, 1981; Röttger et al., 1988; Cho et al., 1992; Rapp and Lübken, 2004; Nicolls et al., 2009; Strelnikova and Rapp, 2010; Latteck and Bremer, 2013; Chau et al., 2018). They are known to be caused due to the presence of ice crystals forming in the region owing to the sharp decrease of temperatures below 150 K, less than the frost point temperature (Rapp and Lübken, 2004; Lübken, 1999; Lübken et al., 2002). The electron density distribution gets affected in an irregular manner due to the charged ice crystals resulting in sharp backscatter several orders of magnitude stronger than the mesospheric turbulent scatter observed in other seasons and lower latitudes. In the case of turbulent scatter, neutral turbulence is expected to

* Corresponding author.
E-mail address: narayananvlwins@gmail.com (V.L. Narayanan).

https://doi.org/10.1016/j.asr.2022.02.015
0273-1177/

reflect in the collision dominated D-region electron densities and cause the weak mesospheric echoes. Uniqueness of PMSE lies in the fact that the presence of ice crystals enables the formation and retention of structures below the scale of turbulent velocity fluctuations and cause significant gradients in the electron densities resulting in intense echoes. The generation of smaller scale turbulent structures is determined by the 'Schmidt number' which increases significantly in the summer polar mesosphere due to the ice formation resulting in a reduction of electron diffusivity extending the lower length scales of turbulent spectrum (Batchelor, 1959; Hill, 1978; Kelley et al., 1987; Cho et al., 1992; Rapp and Lübken, 2003). Noctilucent clouds/ Polar mesospheric clouds are another manifestation of the formation of ice crystals in the summer mesopause altitudes that are related to the PMSE. Noctilucent clouds are believed to be caused by larger ice crystals with sizes above 20 nm while PMSE can occur whenever the electron density distribution is affected by the ice crystals, probably due to their charging. However, their occurrences are not always coincident (Kaifler et al., 2011). In this work, we will focus on the PMSE.

The scattering by PMSE appears to be due to Bragg scatter and hence the observations with a particular frequency in the radio spectrum represents the scale size of the electron density irregularities corresponding to the half wavelength of the incident radio wave (for vertical incidence). Often the PMSE are observed with MST radars in the 50 MHz range. Coordinated multi frequency observations indicate that they are more intense when the radio wavelength is larger within the high frequency limits (Rapp et al., 2008; Strelnikova and Rapp, 2011), and are rare in the ultra high frequencies. Because the presence of ice crystals and their charging creates the PMSE, they are often cited as an example for a dusty plasma phenomenon occurring in nature. Turbulence plays an important role in the creation of the scale sizes that are frozen by the presence of ice crystals even after the velocity eddies disappear. Therefore, in addition to the essential low temperatures, PMSE depend on the background electron density, dust density (i.e. the ice density) and turbulence. Rapp et al. (2008),Varney et al. (2011) showed that the PMSE backscattering depends on the relative amount of dust and electron densities, though without knowing all the three, exact predictions of the PMSE strength becomes cumbersome.

In spite of significant advances in our knowledge about the PMSE phenomenon, their response to different geophysical variations are still under study. In the past, the response of PMSE to geomagnetic activity was studied (Bremer et al., 2000; Zeller and Bremer, 2009; Kirkwood et al., 2013). These works correlated the geomagnetic indices with PMSE power but did not attempt to focus on particle precipitation duration in particular. Though the particle precipitations are related to the geomagnetic activity, comparing the geomagnetic indices does not necessarily indicate response of PMSE to the particle precipitations. This is because the indices like 'ap' are made with the magnetic field changes caused by the currents in the E-region ionosphere. Further, the indices are global in nature. When studying the influence of particle precipitations on PMSE, it is better to study the effect during the particle precipitations preferably in the same spatial region because PMSE is not a spatially uniform feature that can be uniformly observed for 100s of km. To our knowledge, there are few attempts to study the correlations between particle precipitation and PMSE power in a statistical manner (Antonsen and Havnes, 2015; Rauf et al., 2018). Here we undertake a study of response of PMSE spectral parameters, not only power but also the Doppler shift and spectral width, to the particle precipitation events over Ramfjordmoen near Tromsø, Norway. Only a few studies in the past have attempted to focus on the particle precipitation effects on PMSE with this approach like that of Nicolls et al. (2009). The following section discusses the dataset used and methodology adopted. Results are discussed in the Section 3 followed by summary and conclusions in Section 4.

2. Data and Methodology

In this work we study the PMSE spectrum obtained with EISCAT VHF radar located at Ramfjordmoen ($69.6°N, 19.2°E$) near Tromsø, Norway during the summer of 2019. The radar operates with 224 MHz frequency corresponding to the Bragg scale of 67 cm. The radar operation is usually made for a few hours in selected days based on experiment requests from the user groups. Therefore, the data availability is not similar to the MST radars which run continuously for the whole season. Nevertheless, these narrow beam observations in 224 MHz offer valuable insights. The pulse coding used for the PMSE measurements analyzed herein is known as 'Manda' and details of it can be seen from Table 1 (Mann et al., 2016; Tjulin, 2017; Belova et al., 2018). The time and altitude resolutions for these measurements are 4.8 s and 360 m, respectively. We work with the spectrum of the radar echoes at a spectral resolution of 2.604 Hz. We include four successive transmissions to generate a spectrum and hence the tempo-

Table 1
Radar and Experimental parameters.

Frequency	223.4 MHz
Wavelength	1.34 m
Bragg scale	0.67 m
Beam width	$1.2° \times 1.6°$
Peak power	1.2 MW
Transmitted pulse scheme	Manda v4.0
Interpulse period	1.5 ms
Duty cycle	0.098
Time resolution	4.8 s
Range resolution	360 m
Spectral resolution	2.6 Hz
Autocorrelation lag	1.5 ms (pulse to pulse)
Antenna Elevation	90° (zenith)

ral resolution of data used herein is 19.2 s. For our work, we selected days with simultaneous presence of PMSE and particle precipiation reaching below 90 km altitudes during 2019 summer season. The EISCAT radar is co-located with an ionospheric heating facility. Within the available data duration, we have avoided the heating periods because our motivation here is to investigate how the natural particle precipitaions affect the PMSE echoes in cm scales using 224 MHz frequency. Out of 22 days of measurements, 5 days are found to be suitable for the study namely 15, 16, 17 July 2019 and 09 and 10 August 2019. On 15–17 July 2019, there are brief occassions when the ionospheric heater was operated for making conjunctions with SUOMI satellite measurements. These heating periods are removed from our analysis and hence our results are not affected by artificial ionospheric heating effects.

To identify the particle precipitation durations, we used the electron density data obtained from the same VHF radar measurements. The electron densities are obtained from the standard analysis procedure using Grand Unified Incoherent Scatter Design and Analysis package (GUISDAP) software (Lehtinen and Huuskonen, 1996, https://eiscat.se/scientist/user-documentation/guisdap/). In the past, UHF radar measurements are used for electron density information along with the VHF radar measurements of PMSE (e.g. Li and Rapp, 2013). In a previous campaign, the information on electron densities derived from UHF radar data was inconclusive in the presence of PMSE (Mann et al., 2016). Moreover, coordinated UHF observations are not available during our study period. Since we are not focusing on the absolute electron density values at a single height coincident with presence of PMSE, we can identify the enhanced particle precipitation periods with the VHF radar measruements. We consider the values of electron densities measured between 90 and 95 km just above the typical PMSE occurrence regions to estimate the extent of electron density enhancement during particle precipitations. The extension of the particle precipitations to the PMSE heights are visibly clear. The PMSE layers are also identified as high electron density values in the output of standard GUISDAP analysis. However, these are pseudo values indicating an enhanced reflection of the radio waves from the PMSE.

To study PMSE, we need to investigate the Doppler spectrum of the echoes obtained from pulse to pulse correlation in order to have longer auto correlation lags. We use a set of routine known as 'Real Time Graph' (RTG) to obtain such a spectrum (https://doi.org/10.5281/zenodo.4138625). The Doppler spectrum with a frequency resolution of 2.604 Hz between −333 Hz to + 333 Hz is obtained. From the Doppler spectrum, we obtain the three spectral moments by making a Gauss fit to the received spectrum. In the past, Gauss fit is shown to be a good representation for PMSE echoes (Strelnikova and Rapp, 2010; Strelnikova and Rapp, 2011). From the fit, we obtain the peak power, Doppler shift and spectral width. For fitting the Gaussians, we adopt an iterative procedure as below. We select the peak power and its location in the Doppler frequency space. The frequency resolution is taken as the spectral width parameter to start with. The Gauss fitting is made and the root mean square error is calculated with the measured spectrum. Then the fit is optimized to reach minimum root mean square error using Nelder-Mead simplex method. From the optimized Gauss fit curve, the peak power, location of the peak power giving corresponding Doppler frequency and the spectral width parameter are retrieved. The spectral widths given in this work are full width at half maximum (FWHM) of the optimized Gauss fit curves.

Fig. 1 display examples of the Gauss fits made. Note that the y-axis values are different between the panels in the Figure. The fits match the spectra for the peak value very well. Fig. 1(a) shows the PMSE spectrum (black dotted line with stars) with the fitted Gaussian curve (blue dashed line). A vast majority of the PMSE spectra we have investigated both during particle precipitations and other times are similar to Fig. 1(a) in that they are very well represented by the Gauss fit. However, there are few rare intermittent occasions in which the PMSE echoes appear like skewed Gaussian or with multi-peak structures similar to the example in Fig. 1(b). Such occurrences are very few and they are not consistent among adjacent altitudes. For example, if such an occurrence is present in 85 km, the PMSE if present in 85.72 km may be still Gaussian. Moreover, the fitted peak and width closely match with such skewed spectra in many cases we have tested. Therefore, such deviations do not affect the study and we consider the fitted Gaussian parameters such as the peak, location of the peak in the frequency space and its width as the PMSE peak power, Doppler frequency and spectral width, respectively. For simplicity we will often refer to the PMSE peak power as power in this work. The Doppler frequency and spectral width are converted into velocity values by multiplying by 0.67 m, the radar wavelength. Since the Gauss fitting is carried out at all the heights and times, a Gaussian is fit to the maximum value of noise in cases of no PMSE signal. Therefore, we introduce thresholds to the output of fitted parameters in order to retain only the PMSE echoes and remove noise.

After checking several spectra, we fix a threshold power at 0.01 K/Hz above which the echoes are considered as PMSE. It may be noted that the peak of the fit to a noise spectrum lies sometimes at unrealistically large Doppler shifts, for e.g. −100 Hz implying 67 m/s downward Doppler velocity. Such high vertical velocities are unrealistic in the mesosphere. So, in order to remove the noise that overshoots the power threshold, we put another criteria that the Doppler frequencies should be within ±30 Hz corresponding to ±20 m/s vertical velocities. During intense particle precipitations, some noise is still present, probably due to the contribution from incoherent scattering to the spectra from enhanced electron densities along with contamination from intense PMSE echoes in the adjacent range gates. Most of them are removed by applying an

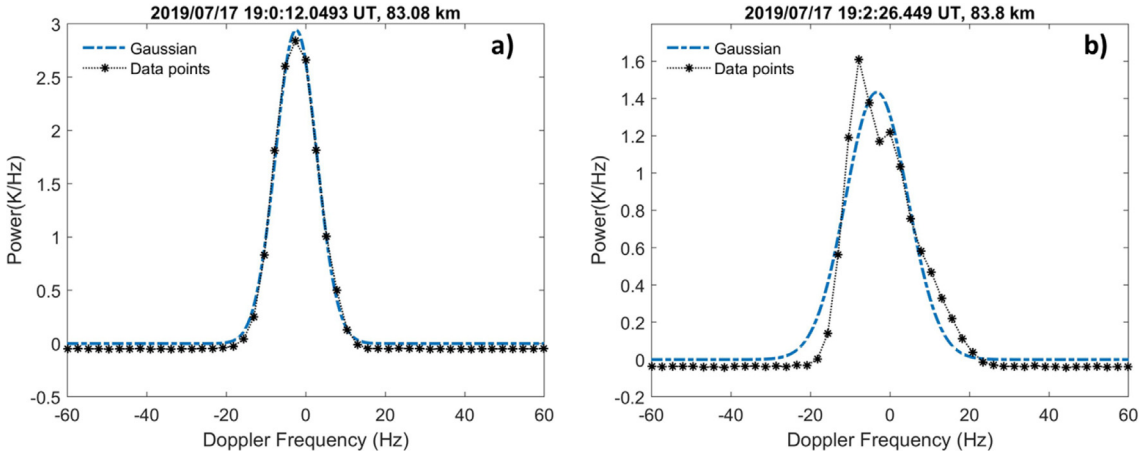

Fig. 1. Samples of spectrum used to identify the PMSE. The black dotted line with stars represent the observed spectrum and the blue dashed line show the optimized Gauss fit. (a) PMSE matching well with Gaussian fit, most frequent case, (b) PMSE showing a skewed Gaussian and double peaked behavior, rare case. Note that y-axis range is different between the panels.

additional threshold to the spectral width such that spectral widths greater than 35 Hz (23.5 m/s) are not considered as PMSE and left out. Therefore, our threshold criteria to retain only PMSE echoes are: (i) peak power of the echo should be greater than 0.01 K/Hz, (ii) Doppler frequency should be below ±30 Hz and (iii) spectral widths should be below 35 Hz. Fig. 2 shows observations from 15 July 2019 without the above mentioned noise thresholds. Fig. 2(a) shows the electron density estimates made by the standard Guisdap procedure. Fig. 2(b), (c) and (d) give the base 10 logarithm of peak power, Doppler velocities with positive values representing upward velocities and spectral widths obtained from the Gauss fits, respectively. Fig. 3 shows the same observations subjected to the threshold conditions. Significant noise reduction may be noticed. We have removed the periods of ionospheric heater operation resulting in white portions (clearly seen in the electron density plots of Fig. 3a).

3. Results and Discussion

Fig. 3 shows the observations on the night of 15 July 2019. The PMSE layer is seen in the region between 83 and 89 km as enhanced electron densities in Fig. 3(a) and in the log(power) shown in Fig. 3(b). During the start of observations around 17:30 UT, multiple weak PMSE layers were present. There were two episodes of particle precipitation on this day as can be seen from the dashed

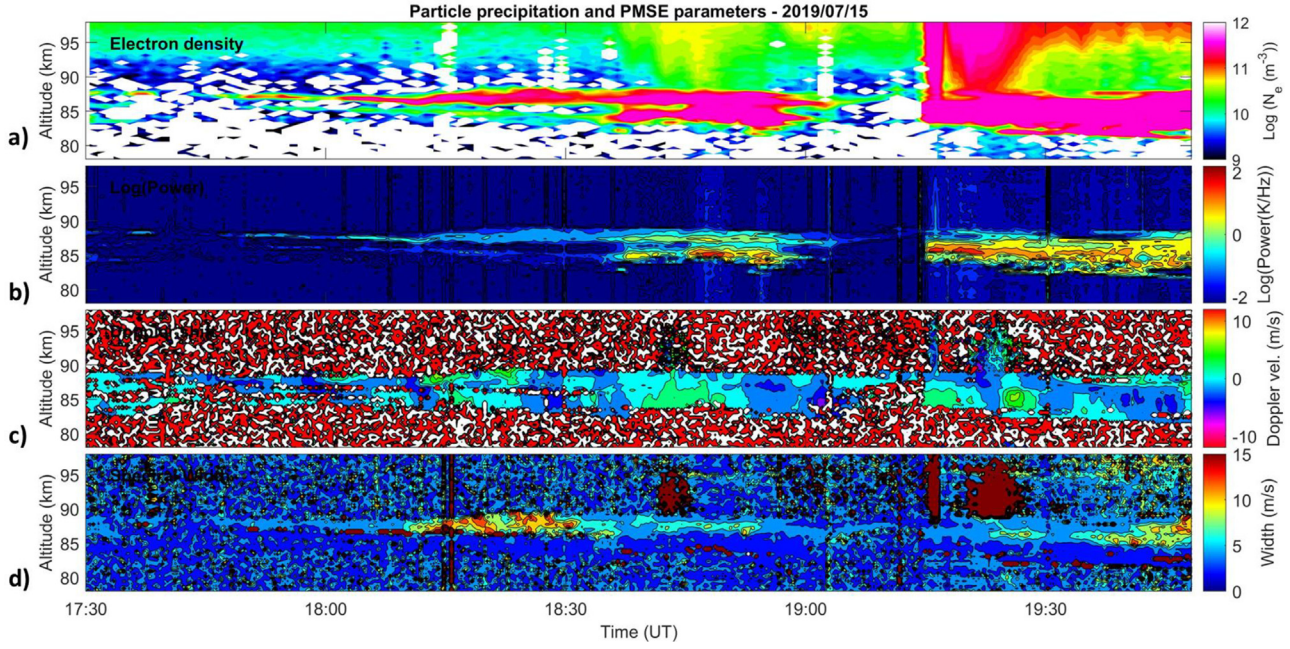

Fig. 2. Observations on 15 July 2019 without applying any noise removal threshold conditions to the Gauss fitting outputs of the spectrum. (a) Electron density estimates using GUISDAP for which the noise thresholds we mentioned did not apply, (b) log(Power (K/Hz)), (c) Doppler velocity (m/s) and (d) Spectral width (m/s) of PMSEs estimated from Gauss fit to the Doppler spectrum.

boxes in the Fig. 3: A moderate level of precipitation from 18:42 UT to 18:55 UT and strong precipitation from 19:15 UT to 19:25 UT that continued with moderate levels of precipitation to the end of observations at 19:46 UT. By strong precipitation, we refer to the periods in which the electron density value increased above $10^{11} electrons/m^3$ around 90 km. By comparing Figs. 3(a) and 3(b), a sudden increase in the power of the PMSE echoes can be noticed in several heights during start of moderate precipitation at 18:42 UT. Within a few minutes after the end of the moderate particle precipitation, both the echo strength and the altitude extent of the echoes decreased considerably. By altitude extent we mean the number of altitude bins where PMSE are identified. The altitude extent of PMSE has reduced below the pre-precipitation levels approximately 10 min after the end of moderate level of precipitation. Again strong particle precipitation has started by 19:15 UT and continued until the end of the observations for the day at 19:46 UT. During this strong particle precipitation the PMSE has increased in its altitude extent and the power of the PMSE was significantly higher.

From Fig. 3(c) it is clear that the Doppler velocities were alternating between positive and negative values of few m/s. Though this magnitude is larger for typical vertical winds expected due to the mesospheric circulation, it should be remembered that these measurements are instantaneous and do not represent the mean background wind. These vertical velocity fluctuations are supposedly result of combination of mean winds, tides, gravity waves and turbulent motion in addition to any bias in the experimental technique (Hoppe and Fritts, 1995; Gudadze et al., 2019). The alternating nature of the velocities indicates probable existance of gravity waves (Fritts et al., 1990; Hoppe and Fritts, 1995). The vertical velocities do not show any response to the particle precipitation events. They appear to alternate between positive and negative values in a similar fashion both before and during the particle precipitation events. This indicates that the particle precipitations does not suddenly alter the vertical winds in the upper mesosphere, which is understandable given that the atmospheric densities are several orders of magnitude higher than the precipitating particles in these altitudes and further the collisions in the neutral gas are significantly higher than that of the electrons.

Fig. 3(d) shows the measured spectral widths that are FWHM of the Gauss fits. Spectral widths are believed to indicate the randomness in the Doppler velocities which is taken as an indication for the turbulence (e.g. Hocking, 1983). For example, if the radar volume is filled with multiple scatterers, their random motion at any instant around the bulk movement contributes to broadening of the spectra which will be measured as spectral width. The bulk motion along the radar beam is measured as Doppler frequency. While there are other sources of spectral broadening, for vertically directed narrow beams as used in this work, the spectral width can be considered as indicator for turbulence (Hocking, 1983; Rapp et al., 2008). From Fig. 3(d), there is no sudden change in the spectral width with respect to the particle precipitation events. However, the spectral widths on this night indicate relatively higher values at upper layers of the PMSE. Initially before 18:35 UT, two layers of PMSE were clear and the spectral widths

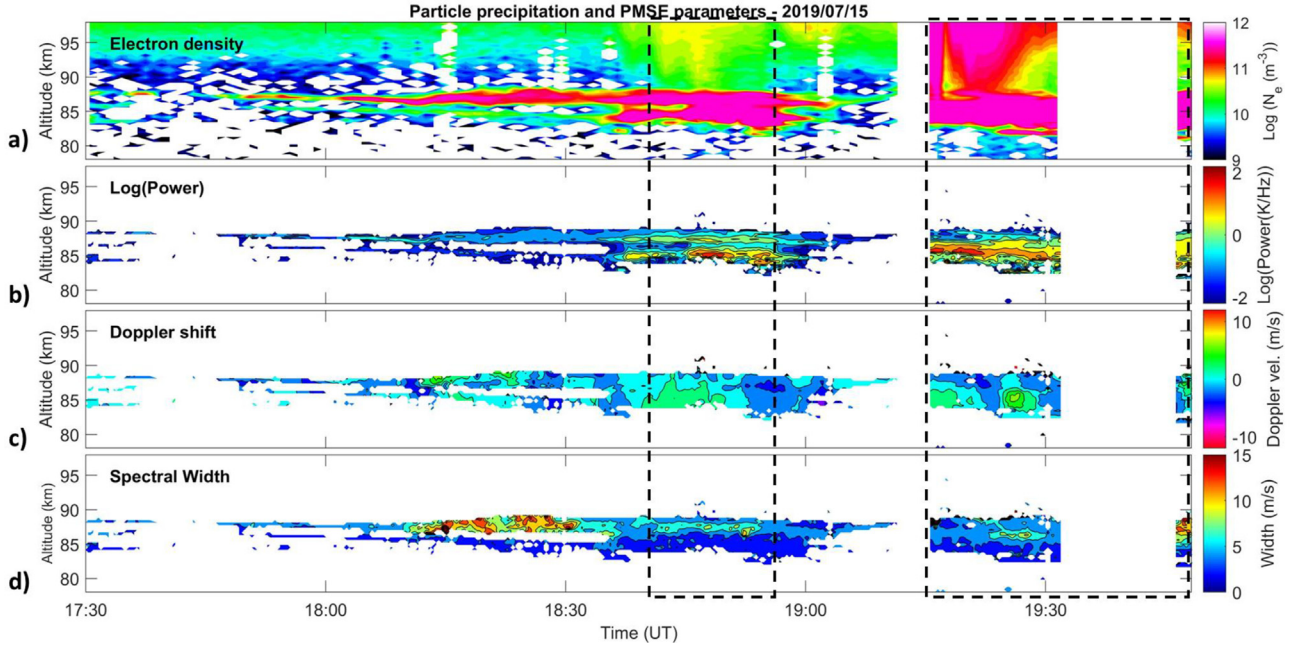

Fig. 3. Observations on 15 July 2019 after applying the noise removal threshold conditions to the Gauss fitting outputs of the spectrum. Note that almost all noise except PMSE are removed. (a) Electron density estimates using GUISDAP for which the noise thresholds we mentioned did not apply, (b) log (Power (K/Hz)), (c) Doppler velocity (m/s) and (d) Spectral width (m/s). The dashed box shows durations of particle precipitation reaching below 90 km.

were higher in the upper layer than the lower layer. After the onset of particle precipitation, the gap region was filled with PMSE as seen from Fig. 3. However, spectral widths were clearly showing two regions.

Right from the early years of identification of PMSE, it is noticed that the spectral widths are not higher in the PMSE regions, though the PMSE is believed to be well related to the turbulence (La Hoz et al., 1989; Röttger and La Hoz, 1990). As explained in the introduction, this is due to the high Schmidt numbers in the region of the PMSE due to the heavier ice particles (Rapp and Lübken, 2003; Rapp and Hoppe, 2006). As a result the electron density in the D-region behaves as a passive tracer to the turbulence and due to high Schmidt numbers, the structures are retained even after the velocity fluctuations fades (Rapp and Lübken, 2003). Such fossil turbulent structures might be more dominant in the high Schmidt number regime. The observation of clear lower spectral width values at the low altitudes might be due to the larger size of the PMSE particles resulting in higher Schmidt numbers and relatively longer retention of turbulent structures in a passive manner. Another interesting aspect to note on this day is that PMSE strength was very high in the regions of lower spectral widths during particle precipitation. This may be clearly seen in the periods from 18:35 to 19:00 and 19:15 to 19:33 UT in Fig. 3(b) and (d).

Fig. 4 shows the results from 16 July 2019 in a similar format to that of Fig. 3. From Fig. 4(a) two particle precipitation events of moderate intensity can be identified to extend below 90 km into the PMSE region. The first one was from 20:00 to 20:22 UT and the second one started at 20:52 UT and continued until the end of observations at 20:59 UT. On this day PMSE occurred only above 84 km and below 89 km. The small patches seen below 84 km in Fig. 4(b)-(d) occur during particle precipitation probably due to incoherent scattering contribution resulting from enhanced electron densities. Another possibility is that there may be structures contributing to the lower altitude mesospheric echoes which become observable during particle precipitations. Lower mesospheric altitude echoes are observed occassionally as discussed in Latteck et al. (2021). However, they do not appear to be PMSE echoes and hence we label them as 'false positive detections' that satisfy our threshold criteria. The region of false detections of PMSE is shown by a gray box in Fig. 4(b). From Fig. 4(b), it can be noted that there is a slight increase in the number of altitudes in which PMSE occurred along with an increase in the power of the echoes at the middle of the layer between 20:00 and 20:22 UT. After this precipitation event, there is a sudden absence of PMSE for a couple of minutes and then PMSE resumed with a reduced power at pre-event levels. Around 20:30 UT, the intensity of PMSE has suddenly increased without any clear particle precipitations extending below 90 km. This increase might be due to the wind bringing in PMSE structures from area outside the radar beam. If the enhancement is due to the onset of active turbulence, some enhancement is expected to be seen in the spectral widths irrespective of magnitude of Schmidt numbers. Lack of sudden change in the spectral widths shown in Fig. 4(d) supports the possibility of advection of PMSE structures into the radar beam by the horizontal winds. Even if the larger ice particles were causing the PMSE, an active turbulence is expected to be revealed in the spectral widths,

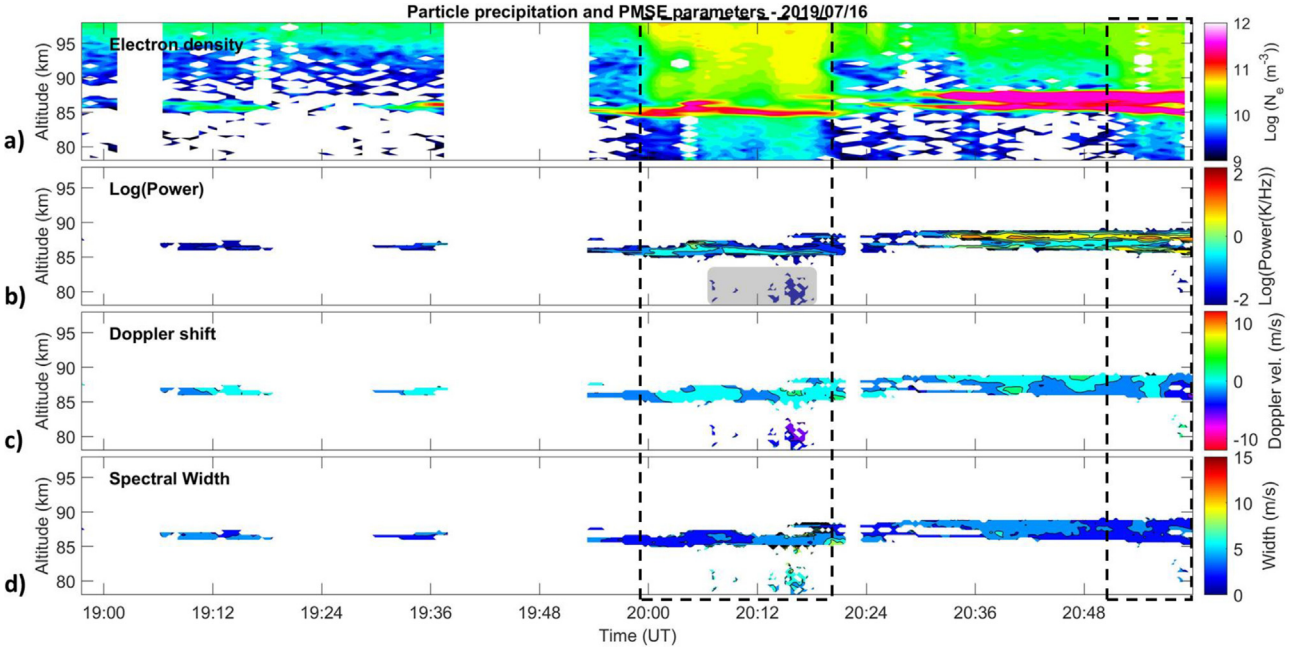

Fig. 4. Observations on 16 July 2019 in the same format as Fig. 3. The dashed box shows duration of particle precipitation and the gray region in Fig. 4(b) shows false detections of PMSE, probably due to the incoherent scatter contribution during enhanced particle precipitation or due to existence of lower altitude structures giving rise to echoes similar to lower altitude mesospheric echoes (see text for details).

which was not the case around 20:30 UT. Similar to the observations on 15 July 2019, there is no sudden change in the vertical velocities and spectral widths following the particle precipitation events (Fig. 4(b) and (d)). Only the power and altitude extent of the PMSEs appear to vary with the particle precipitation events.

Fig. 5 shows the observations on 17 July 2019 in the same format as Figs. 3 and 4. On this day, there was a moderate level of particle precipitation right from the start of the radar observations at 18:56 UT to 19:25 UT as can be seen from Fig. 5(a). Afterwards the ionosphere was quiet without particle precipitation until the end of the observations at 20:57 UT. Fig. 5(b) displays that the PMSE altitude extent and the power were both higher during the particle precipitation duration. Fig. 5(c) shows that the Doppler velocities are within few m/s, mostly upward on this day. However the values are similar to the previous cases. Fig. 5(d) show two regions with clearly different spectral width values. The PMSE below 85 km have higher spectral widths than those between 85 and 90 km region. This is particularly intense during the particle precipitation. This behaviour is opposite to that of 15 July 2019 wherein the upper part of the PMSE layer was having higher spectral widths. At the same time, it is worth noting that the power of the PMSE was relatively higher in the regions of lesser spectral width during the particle precipitations. Later on, we will investigate this behaviour on all the days considered herein.

Another interesting feature from 17 July 2019 observations is the formation of thin layers of PMSE just above 90 km. These PMSE occur after the particle precipitation period and were intermittent in nature. They occur between 89 and 92 km. The spectral widths during these events were clearly higher indicating possibility of active turbulence generating these higher altitude PMSE (compare Fig. 5 (b) and (d)). Note that these PMSE formed before the ionospheric heater was on at 19:29 UT. A white gap region is seen in all the panels of Fig. 5 indicating periods of ionospheric heating experiment. Therefore, the initiation of these PMSE were neither due to particle precipitation nor due to artificial ionospheric heating. The active turbulence possibility is supported by co-occurrence of higher spectral widths.

Fig. 6 shows the observations on the night of 09 August 2019 from 20:00 UT to 02:00 UT on 10 August 2019. Fig. 6 (a) shows existence of multiple particle precipitation durations marked by dashed boxes. The first one started from about 20:06 UT and lasted until 21:10 UT with a small dip in precipitation for a couple of minutes around 20:40 UT. There was a very short duration precipitation for about 4 min from 21:15 to 21:19 UT. From 22:25 to 23:00 UT, there was a sudden decrease in the particle precipitation. This is not an experimental artifact. There seems to be a sudden and sharp decrease in the particle precipitation which is confirmed by comparing the E- and F-region measurements up to 209 km that are not shown here.

From Fig. 6(b), the intensification of PMSE power may be inferred during particle precipitation between 20:06 UT and 21:10 UT. Such intensification was noticed even for the short duration precipitation between 21:15 and 21:19 UT. In addition to the intensification of the power, the number of altitudes in which PMSE has occurred has increased as will be discussed later. PMSE disappeared at 22:37 UT, around 10 min after the sudden decrease in the precipitation. The echoes below 85 km between 20:45 and 21:00 UT are due to false detections of PMSE as indicated by the gray area in Fig. 6(b). Similar to 16 July 2019, it may be seen to correspond to the extension of the particle pre-

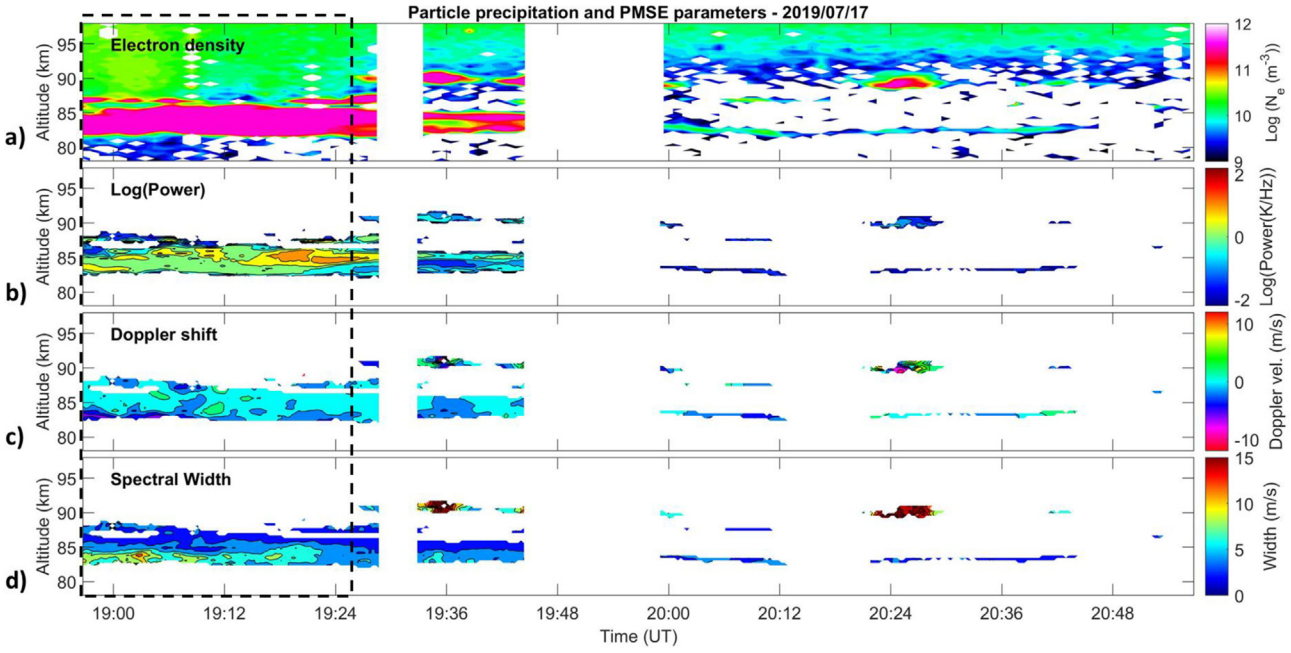

Fig. 5. Observations on 17 July 2019 in the same format as Fig. 3. The box shows the duration of particle precipitation.

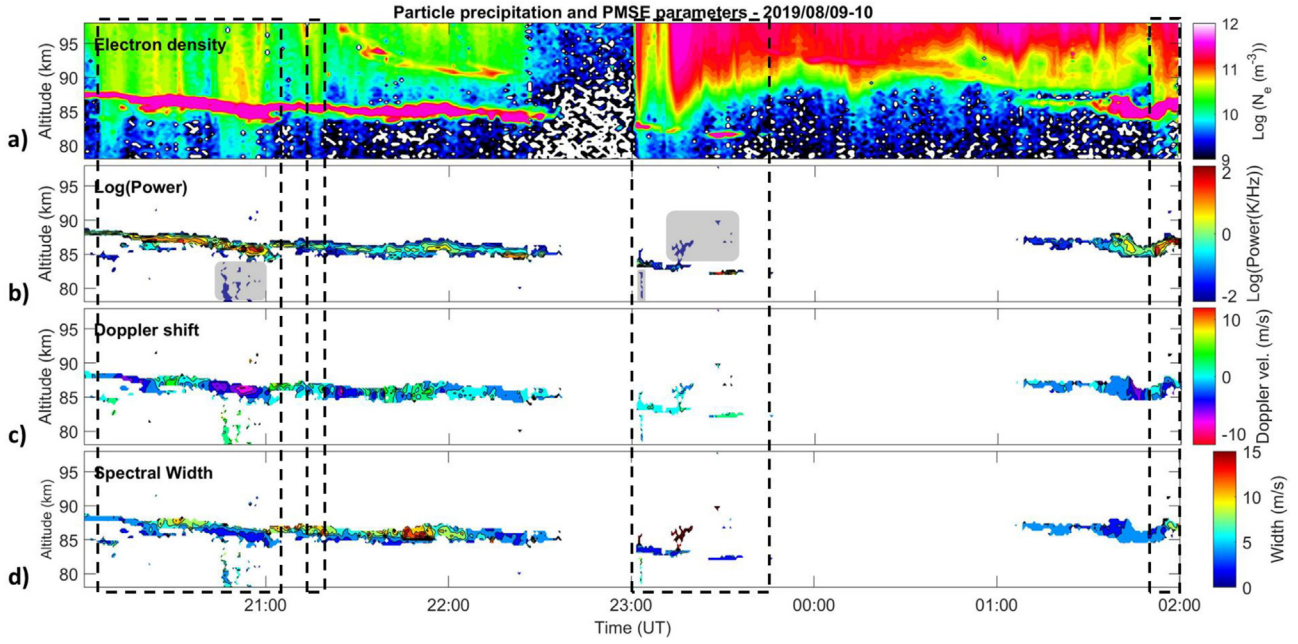

Fig. 6. Observations on 09/10 August 2019 in the same format as Fig. 3. The dashed boxes and gray regions represent duration of particle precipitation and false PMSE detections, respectively.

cipitation to lower altitudes by comparing Fig. 6(a) and (b). Therefore, they may be either due to incoherent scattering contribution from sudden enhancement in electron density or due to the lower altitude mesospheric echoes.

Intense particle precipitation has restarted from 23:00 UT on 9 August 2019 and lasted until the end of observations at 02:00 UT on 10 August 2019. Within this period, during 23:00 to 23:41 UT on 9 August and 01:50 to 02:00 UT on 10 August, the particle precipitation has further descended to lower altitudes. PMSE has also restarted along with the strong precipitation at 23:00 UT. PMSE was present from 23:00 to 23:18 UT, 23:25 to 23:35 UT on 9 August and 01:09 to 02:00 UT on 10 August. Though the power of restarted PMSE was weaker in the duration between 23:00 and 23:30 UT, it is important to note their re-occurrence along with onset of the intense particle precipitation. In the duration between 23:15 and 23:30 some false PMSE detections are also noticed during intense precipitation as marked by the gray area in Fig. 6(b). The particle precipitation below 90 km altitudes was weakening after 23:18 UT and coincidentally there was disappearance of the weak PMSE around that time. Again PMSE formed for 10 min between 23:25 and 23:35 UT with a slight enhancement of particle precipitation in the lower altitudes (see Fig. 6(a) and (b)). There was another sudden enhancement in the particle precipitation well below 85 km from 01:50 to 02:00 UT which was continuing but observations were stopped. PMSE was already present by this time but there was an enhancement in the power.

On this night the vertical velocities showed a similar behaviour of the other days with alternating positive and negative velocities of few m/s magnitudes without any noticeable response to the particle precipitations (see Fig. 6(c)). Spectral widths shown in Fig. 6(d) indicates relatively higher values at times. However, a closer examination shows that the higher spectral widths occurred only at the upper part of the PMSE layer on this night.

The events presented above show that a clear response to the particle precipitation is seen only in the power of the PMSE echoes and in the altitude extent of their occurrence. The Doppler shifts associated with the vertical velocities and the spectral widths associated with the turbulence do not respond to particle precipitations. We check if there is a functional form of relationship between the electron density enhancements during particle precipitations and increases in PMSE peak power and altitude extent. We select three minute duration before and during the particle precipitation events and compare the normalized changes of the parameters according Eq. 1. Three minute duration are selected in order to keep the duration of comparison equal between precipitation and no-precipitation.

$$P_{dif} = \frac{P_{pre} - P_{nor}}{P_{pre}} \tag{1}$$

where, P_{dif} represents the normalized change in the parameters. The parameters being average electron density between 90 and 95 km, total sum of PMSE peak power between 80 and 90 km and altitude extent of PMSE quantified as the number of observations of PMSE/total number of measurement bins within the three minute duration between 80 and 90 km. P_{pre} is the value of the parameter during particle precipitation and P_{nor} is the value without particle precipitation measured few minutes before the onset of particle precipitation. Only on 17 July 2019, we

Table 2
Measured parameters in the selected durations with and without particle precipitation.

Date	Without particle precipitation				With particle precipitation				Normalized change (Eq. 1)		
	Time (UT)	Electron density $\times 10^9 (m^{-3})$	Sum of PMSE peak power	PMSE extent (No. of PMSE bins/ Total No. of bins)	Time (UT)	Electron density $\times 10^9 (m^{-3})$	Sum of PMSE peak power	PMSE extent (No. of PMSE bins/ Total No. of bins)	Electron density	PMSE power	PMSE extent
15/07	18:33–18:36	8.69	15.83	0.48	18:48–18:51	33.47	977.52	0.52	0.74	0.98	0.09
15/07	19:06–19:09	12.93	0.89	0.1	19:18–19:21	285.35	1392.07	0.53	0.95	1	0.81
16/07	19:54–19:57	6.57	3.26	0.14	20:06–20:09	50.24	19.64	0.32	0.87	0.83	0.55
16/07	20:42–20:45	15.65	190.25	0.30	20:55–20:58	40.51	246.77	0.37	0.61	0.23	0.17
17/07	19:39–19:42	7.68	38.62	0.32	19:15–19:18	17.26	398.61	0.51	0.56	0.9	0.37
09/08	20:01–20:04	11.64	16.39	0.15	20:07–20:10	38.96	33.21	0.27	0.7	0.51	0.44
09/08	22:48–22:51	3.08	0	0	23:03–23:06	69.91	16.14	0.2	0.96	1	1
10/08	01:45–01:48	37.04	26.67	0.2	01:54–01:57	138.83	233.56	0.28	0.73	0.89	0.29

measure P_{nor} in the quiet period after the particle precipitation because particle precipitation was present from the start of VHF observations on the day. Eq. 1 is such that the maximum value of P_{dif} can be 1, a value of 0 indicates no change in the parameter during particle precipitation and negative values indicate a decrease in the value of the parameter during particle precipitation. A value of 1 indicates that the PMSE was absent before particle precipitation and the parameter has been observed with the onset of particle precipitation. Note from Figs. 3–6 that nine particle precipitation durations are highlighted. Among them we select eight cases leaving the short particle precipitation burst from 21:15 to 21:19 UT on 9 August 2019. We leave that event because the previous particle precipitation lasted until five minutes before this burst of precipitation occurred. The selected three minute durations, absolute value of the parameters and their normalized changes are shown in the Table 2.

The normalized change in PMSE power and altitude extent with respect to the change in the electron density during particle precipitations are given in Fig. 7. Note that all the values are positive indicating that the PMSE power and altitude extent certainly increases with an increase in electron density during particle precipitations. However, the scatter plot readily indicates lack of linear or any other simple functional form of relationship between the parameters. This confirms the findings of the earlier works that PMSE strength depend not only on electron density but also on other parameters like ice density (Rapp et al., 2008; Nicolls et al., 2009; Varney et al., 2011).

On the other hand, within the PMSE layer the spectral widths often reveal presence of two regions separated in altitude. On 15 July and 09/10 August, the upper part of the layer was of predominantly higher spectral width while on 17 July the lower part was of higher width. This behaviour is seen irrespective of particle precipitation. We propose that this might be the result of active turbulence acting on lighter particles along with heavier particles causing the PMSE in higher Schmidt number regime wherein the actual turbulence velocity eddies are decaying. However, why there is a sharp separation in spectral widths instead of a gradual variation is unclear and requires further experiments with supporting information like temperature and ice density which we lack at present.

We have also noticed from Figs. 3 and 5 that there was an inverse relation between the PMSE peak power and spectral widths during particle precipitation periods. In order to investigate this, we use data during the same three minute periods given in Table 2. In Fig. 8, we plot the power and corresponding spectral widths without and with particle precipitation. Note that the x-axis limits are different between Fig. 8(a) and (b). In order to have nearly same amount of data points we decided to carryout the analysis for the same three minute intervals given in Table 2. Fig. 8 (a) and (b) clearly shows that irrespective of the presence of particle precipitation, the high power echoes almost always

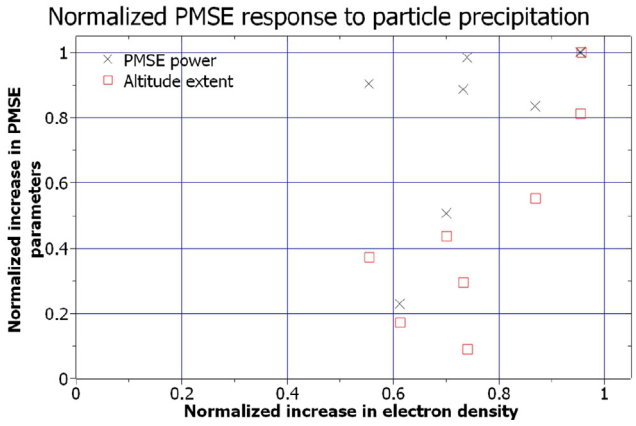

Fig. 7. Response of PMSE power and altitude extent to the electron density enhancements due to particle precipitation. All the parameters are normalized according to Eq. 1 (see text for details).

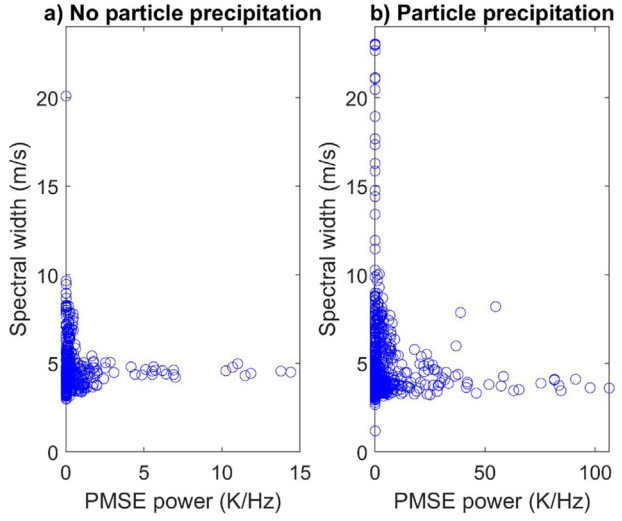

Fig. 8. PMSE power vs. spectral width. (a) quiet time without particle precipitation, (b) during particle precipitation.

occurred with moderate to low level of spectral widths within 6 m/s of full width at half maximum. The converse also appears to be correct in that high spectral width values almost always accompany very weak PMSE echoes. We remind that the power threshold we kept for PMSE detection is 0.01 K/Hz and hence the crowded points near the 0 indicates weak PMSE echoes. Earlier, Rapp and Hoppe (2006) showed an anticorrelation between the power and spectral width at some particular heights. Here we show that this appears to be a general behaviour. We have noticed this behaviour on some other cases as well and planning for a detailed analysis in the future.

The enhancement in the peak power of PMSE during particle precipitation is clearly revealed in Fig. 8. While spectral widths did not show a sudden response in Figs. 3–6, Fig. 8 show that there are many points with higher spectral widths during particle precipitation. This might be explained if the significant enhancements of power are caused by larger particles that are present in high Schmidt number region with weak spectral width components. The larger particles may be more effective in getting charged when electron density increases, thereby affecting the electron density gradient and resulting in stronger echoes. The sporadic enhancements in the spectral widths during particle precipitations revealed from Fig. 8 may be due to the enhancement in electron density enabling increased echoes from small sized particles existing in turbulent regions. Therefore, in both the cases it appear as if the enhanced electron densities 'lits' the preexisting dormant Bragg scale structures of PMSE. This is also supported by preexistence of weak PMSE before the particle precipitations in many of the cases. At the same time, the other possibility for the sporadic enhancements in the spectral widths during particle precipitation may be from the contribution from incoherent scattering due to the enhanced electron densities in the regions of weak PMSE. Though our results are based on Gauss fitting, incoherent scattering is known to be represented by Lorentzian form in the D-region heights (e.g. (Chau and Kudeki, 2006)). When the PMSE are weak, sudden enhancement of electron densities would have affected the widths of the Gauss fits due to broadening from incoherent scattering. While this can explain the sporadic enhancement in the high spectral width weak PMSE during particle precipitation events, the very existence of weak PMSE structures with relatively larger spectral widths in the normal conditions without any electron density enhancements demand a detailed study in the future.

4. Summary and conclusion

In this work we have carried out detailed investigation on the response of the PMSE to the particle precipitation events. Gauss fitting is made to the PMSE spectra and the parameters of peak power, Doppler velocity and FWHM Spectral widths are obtained. Five days of EISCAT VHF radar data at 224 MHz from July and August 2019 were studied. Standard Guisdap analyzed electron density measurements between 90 and 95 km are considered as proxy for particle precipitations. The results showed clear response only in the power and altitude extent of the PMSE echoes during particle precipitation events.

It is important to note that the very existence of PMSE is not related to the particle precipitations. Other factors like the existence of temperatures below frost point, enough water vapor, turbulent structures and wind advection of the structures within radar beam are important along with the electron density. There are occasions in which PMSE has suddenly started (19:30 UT on 16 July and 01:09 UT on 10 August, for example) or its power has increased without any correspondence to the increase in the particle precipitations (20:30 UT on 16 July, for example). Nevertheless, PMSE power has shown an increase with particle precipitations in all the cases studied herein including a short burst of precipitation (on 9 August

2019 between 21:15–21:19 UT). The altitude extent of PMSE often increased during precipitations (see Fig. 7 and Table 2) and that was the case particularly for intense particle precipitations. Often the lower portion of the PMSE layer appears to extend resulting in an increased altitude extent with particle precipitations. There are also occasions wherein PMSE started suddenly with onset of particle precipitations (23:00 UT on 9 August). However, there is no simple functional form of relationship between the electron density enhancements and the increase in the power of the echoes during particle precipiation events. This is in concurrence with previous studies. The Doppler vertical velocities and the spectral widths did not show any abrupt variations associated with the particle precipitations.

These observations indicate that the dormant structures already existing in the region are immediately converted into active scatterers by the sudden influx of electrons during particle precipitation events. Such an interpretation also explains sudden formation of PMSE on certain altitudes during the onset of particle precipitations. The lack of linear relationships might be due to the variabilities in the other controlling factors like amount of ice crystals, extent of dormant structures and temperature as mentioned above.

Apart from the influence of particle precipitations, an inverse relationship between spectral widths and PMSE peak power is noticed such that the high power reflections almost always contain moderate to weak spectral widths. This inverse relationship appears to intensify during particle precipitation cases in that both the number of high power echoes and high spectral width points increased compared with quiet periods. Though incoherent scattering contribution from the enhanced electron densities during particle precipitations may have contributed to broader spectral widths of weak PMSE, existence of such an inverse relationship in the absence of particle precipitations is noteworthy. A detailed study on this inverse relationship is planned for future work.

Declaration of Competing Interest

The authors declare that they have no known competing financial interests or personal relationships that could have appeared to influence the work reported in this paper.

Acknowledgments

This research has been supported by the Research Council of Norway (Grant No. NFR 275503). The data utilized in this work are collected and distributed by EISCAT scientific Association. EISCAT is an international association supported by research organisations in China (CRIRP), Finland (SA), Japan (NIPR and ISEE), Norway (NFR), Sweden (VR), and the United Kingdom (UKRI). The analyzed data and the spectra used in this work can be obtained from https://doi.org/10.18710/YSDZF8 (Narayanan, 2021).

References

Antonsen, T., Havnes, O., 2015. On the relationship between pmse strength and particle precipitation. In: Proc. '22nd ESA Symposium on European Rocket and Balloon Programmes and Related Research', Tromsø Norway, 7–12 June 2015. European Space Agency. URL: https://hdl.handle.net/10037/8607.

Batchelor, G.K., 1959. Small-scale variation of convected quantities like temperature in turbulent fluid part 1. general discussion and the case of small conductivity. J. Fluid Mech. 5 (1), 113–133. https://doi.org/10.1017/S002211205900009X.

Belova, E., Kawnine, M., Häggström, I., Sergienko, T., Kirkwood, S., Tjulin, A., 2018. Tristatic observation of polar mesosphere winter echoes with the eiscat vhf radar on 8 january 2014: a case study. Earth, Planets and Space 70 (1), 1–12.

Bremer, J., Hoffmann, P., Hansen, T., 2000. Geomagnetic control of polar mesosphere summer echoes. Ann. Geophys. 18 (2), 202–208.

Chau, J.L., Kudeki, E., 2006. First e- and d-region incoherent scatter spectra observed over jicamarca. Ann. Geophys. 24 (5), 1295–1303. https://doi.org/10.5194/angeo-24-1295-2006.

Chau, J.L., McKay, D., Vierinen, J.P., La Hoz, C., Ulich, T., Lehtinen, M., Latteck, R., 2018. Multi-static spatial and angular studies of polar mesospheric summer echoes combining maarsy and kaira. Atmos. Chem. Phys. 18 (13), 9547–9560. https://doi.org/10.5194/acp-18-9547-2018.

Cho, J.Y.N., Hall, T.M., Kelley, M.C., 1992. On the role of charged aerosols in polar mesosphere summer echoes. J. Geophys. Res.: Atmos. 97 (D1), 875–886. https://doi.org/10.1029/91JD02836.

Czechowsky, P., Ruester, R., Schmidt, G., 1979. Variations of mesospheric structures in different seasons. Geophys. Res. Lett. 6 (6), 459–462. https://doi.org/10.1029/GL006i006p00459.

Ecklund, W.L., Balsley, B.B., 1981. Long-term observations of the arctic mesosphere with the mst radar at poker flat, alaska. J. Geophys. Res.: Space Phys. 86 (A9), 7775–7780. https://doi.org/10.1029/JA086iA09p07775.

Fritts, D., Hoppe, U.-P., Inhester, B., 1990. A study of the vertical motion field near the high-latitude summer mesopause during mac/sine. J. Atmos. Terrestr. Phys. 52 (10–11), 927–938.

Gudadze, N., Stober, G., Chau, J.L., 2019. Can vhf radars at polar latitudes measure mean vertical winds in the presence of pmse? Atmos. Chem. Phys. 19 (7), 4485–4497.

Hill, R.J., 1978. Nonneutral and quasi-neutral diffusion of weakly ionized multiconstituent plasma. J. Geophys. Res. 83 (A3), 989–998. https://doi.org/10.1029/JA083iA03p00989.

Hocking, W., 1983. On the extraction of atmospheric turbulence parameters from radar backscatter doppler spectra–i. theory. J. Atmos. Terr. Phys. 45 (2–3), 89–102.

Hoppe, U.-P., Fritts, D.C., 1995. High-resolution measurements of vertical velocity with the european incoherent scatter vhf radar: 1. motion field characteristics and measurement biases. J. Geophys. Res.: Atmos. 100 (D8), 16813–16825.

Kaifler, N., Baumgarten, G., Fiedler, J., Latteck, R., Lübken, F.-J., Rapp, M., 2011. Coincident measurements of pmse and nlc above alomar (69° n, 69° e) by radar and lidar from 1999–2008. Atmos. Chem. Phys. 11 (4), 1355–1366. https://doi.org/10.5194/acp-11-1355-2011.

Kelley, M.C., Farley, D.T., Röttger, J., 1987. The effect of cluster ions on anomalous vhf backscatter from the summer polar mesosphere. Geophys. Res. Lett. 14 (10), 1031–1034. https://doi.org/10.1029/GL014i010p01031.

Kirkwood, S., Belova, E., Dalin, P., Mihalikova, M., Mikhaylova, D., Murtagh, D., Nilsson, H., Satheesan, K., Urban, J., Wolf, I., 2013. Response of polar mesosphere summer echoes to geomagnetic disturbances in the southern and northern hemispheres: the importance of nitric oxide. Ann. Geophys. 31 (2), 333–347.

La Hoz, C., Röttger, J., Franke, S., 1989. Dynamic spectra of pmse measured by eiscat at 224 mhz. Middle Atmosphere Program. Handbook for MAP volume 28, 28, 248.

Latteck, R., Bremer, J., 2013. Long-term changes of polar mesosphere summer echoes at 69n. J. Geophys. Res.: Atmos. 118 (18), 10441–10448. https://doi.org/10.1002/jgrd.50787.

Latteck, R., Renkwitz, T., Chau, J.L., 2021. Two decades of long-term observations of polar mesospheric echoes at 69n. J. Atmos. Solar Terr. Phys. 216, 105576. https://doi.org/10.1016/j.jastp.2021.105576.

Lübken, F.-J., 1999. Thermal structure of the arctic summer mesosphere. J. Geophys. Res.: Atmos. 104 (D8), 9135–9149. https://doi.org/10.1029/1999JD900076.

Lehtinen, M.S., Huuskonen, A., 1996. General incoherent scatter analysis and guisdap. J. Atmos. Terr. Phys. 58 (1–4), 435–452.

Li, Q., Rapp, M., 2013. PMSE observations with the EISCAT VHF- and UHF-radars: Ice particles and their effect on ambient electron densities. J. Atmos. Solar Terr. Phys. 104, 270–276. https://doi.org/10.1016/j.jastp.2012.10.015.

Lübken, F.-J., Rapp, M., Hoffmann, P., 2002. Neutral air turbulence and temperatures in the vicinity of polar mesosphere summer echoes. J. Geophys. Res. (Atmos.) 107 (D15), 4273. https://doi.org/10.1029/2001JD000915.

Mann, I., Häggström, I., Tjulin, A., Rostami, S., Anyairo, C.C., Dalin, P., 2016. First wind shear observation in pmse with the tristatic eiscat vhf radar. J. Geophys. Res.: Space Phys. 121 (11), 11271–11281. https://doi.org/10.1002/2016JA023080.

Narayanan, V.L., 2021. Replication data for 'Effects of particle precipitation on the polar mesospheric summer echoes observed by EISCAT VHF 224 MHz radar', DataverseNO, V1. https://doi.org/10.18710/YSDZF8.

Nicolls, M.J., Kelley, M.C., Varney, R.H., Heinselman, C.J., 2009. Spectral observations of polar mesospheric summer echoes at 33cm (450mhz) with the poker flat incoherent scatter radar. J. Atmos. Solar Terr. Phys. 71 (6), 662–674. https://doi.org/10.1016/j.jastp.2008.04.019.

Rapp, M., Hoppe, U.-P., 2006. A reconsideration of spectral width measurements in pmse with eiscat. Adv. Space Res. 38 (11), 2408–2412.

Rapp, M., Lübken, F.-J., 2003. On the nature of pmse: Electron diffusion in the vicinity of charged particles revisited. J. Geophys. Res.: Atmos. 108 (D8). https://doi.org/10.1029/2002JD002857.

Rapp, M., Lübken, F.-J., 2004. Polar mesosphere summer echoes (pmse): Review of observations and current understanding. Atmos. Chem. Phys. 4 (11/12), 2601–2633. https://doi.org/10.5194/acp-4-2601-2004.

Rapp, M., Strelnikova, I., Latteck, R., Hoffmann, P., Hoppe, U.-P., Häggström, I., Rietveld, M.T., 2008. Polar mesosphere summer echoes (pmse) studied at bragg wavelengths of 2.8m, 67cm, and 16cm. J. Atmos. Solar-Terrestrial Phys., 70(7), 947–961. doi: 10.1016/j.jastp.2007.11.005.

Rauf, A., Li, H., Ullah, S., Meng, L., Wang, B., Wang, M., 2018. Statistical study about the influence of particle precipitation on mesosphere summer echoes in polar latitudes during July 2013. Earth, Planets and Space 70 (1), 1–13.

Röttger, J., La Hoz, C., 1990. Characteristics of polar mesosphere summer echoes (pmse) observed with the eiscat 224 mhz radar and possible explanations of their origin. J. Atmos. Terrestr. Phys. 52 (10–11), 893–906.

Röttger, J., La Hoz, C., Kelley, M.C., Hoppe, U.-P., Hall, C., 1988. The structure and dynamics of polar mesosphere summer echoes observed with the eiscat 224 mhz radar. Geophys. Res. Lett. 15 (12), 1353–1356. https://doi.org/10.1029/GL015i012p01353.

Strelnikova, I., Rapp, M., 2010. Studies of polar mesosphere summer echoes with the EISCAT VHF and UHF radars: Information contained in the spectral shape. Adv. Space Res. 45 (2), 247–259. https://doi.org/10.1016/j.asr.2009.09.007.

Strelnikova, I., Rapp, M., 2011. Majority of PMSE spectral widths at UHF and VHF are compatible with a single scattering mechanism. J. Atmos. Solar Terr. Phys. 73 (14–15), 2142–2152. https://doi.org/10.1016/j.jastp.2010.11.025.

Tjulin, A., 2017. Eiscat experiments. EISCAT Scientific Association, (March),. URL: https://eiscat.se/wp-content/uploads/2017/04/Experiments.pdf.

Varney, R.H., Kelley, M.C., Nicolls, M.J., Heinselman, C.J., Collins, R. L., 2011. The electron density dependence of polar mesospheric summer echoes. J. Atmos. Solar Terr. Phys. 73 (14), 2153–2165. https://doi.org/10.1016/j.jastp.2010.07.020.

Zeller, O., Bremer, J., 2009. The influence of geomagnetic activity on mesospheric summer echoes in middle and polar latitudes. Ann. Geophys. 27 (2), 831–837.